Supporting Information

Photocytotoxicity and Photoinduced Phosphine Ligand Exchange in a Ru(II) Polypyridyl Complex

Sean J. Steinke,[‡] Sayak Gupta,[†] Eric J. Piechota,[‡] Curtis E. Moore,[‡] Jeremy J. Kodanko,[†]* and Claudia Turro[‡]*

[‡]*Department of Chemistry and Biochemistry, The Ohio State University, Columbus, OH 43210*

[†]*Department of Chemistry, Wayne State University, Detroit, MI 48208*

*Corresponding Authors: turro.1@osu.edu; jkodanko@wayne.edu

Table of Contents **Page Number**

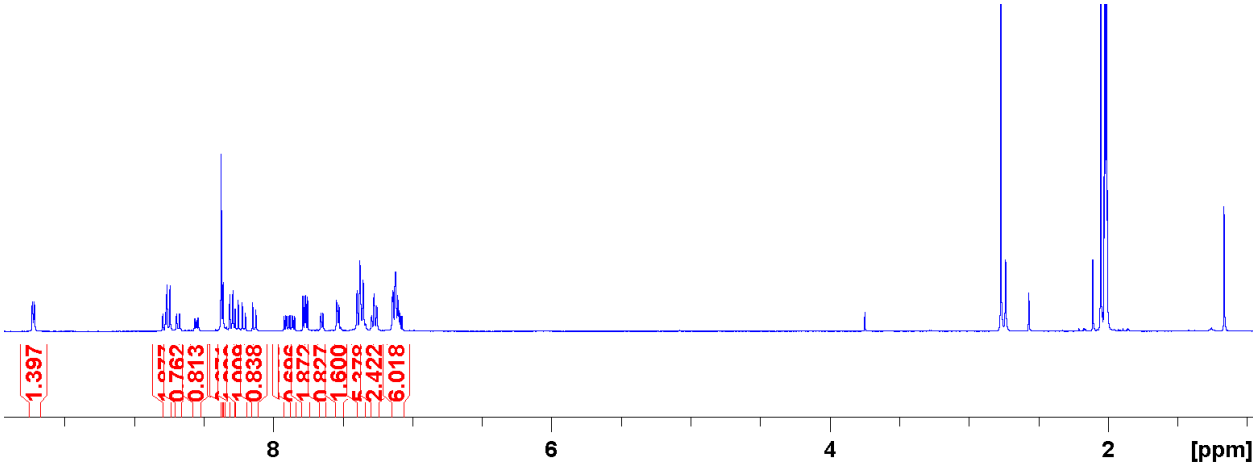

Figure S1. ^{1}H NMR spectrum of $[Ru(phen)_2(PPh_3)Cl]^+$ in $(CD_3)_2CO$.

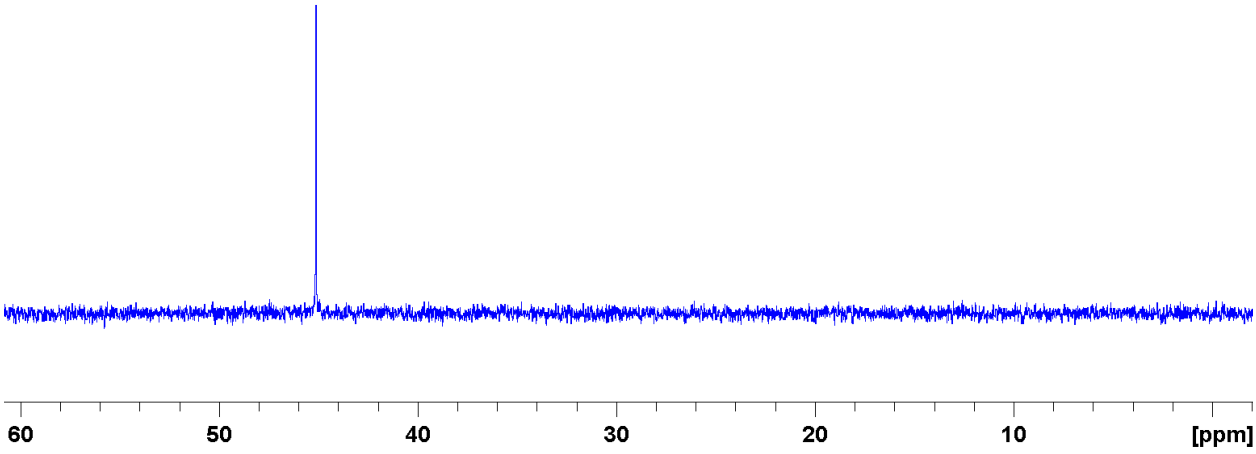

Figure S2. $^{31}P\{H\}$ NMR spectrum of $[Ru(phen)_2(PPh_3)Cl]^+$ in $(CD_3)_2CO$.

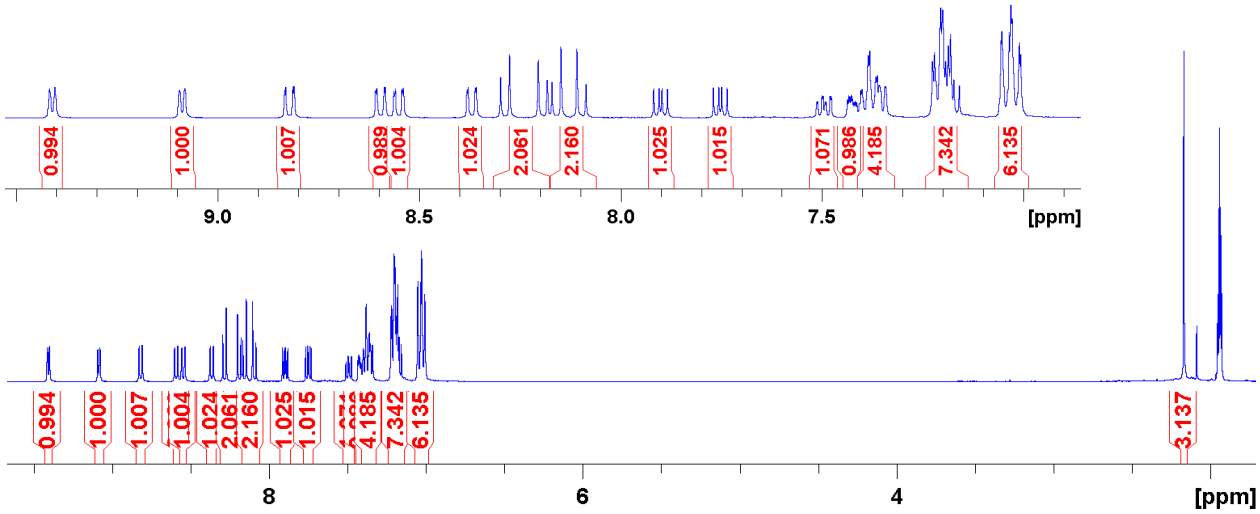

Figure S3. ^{1}H NMR of **1a** in CD_3CN.

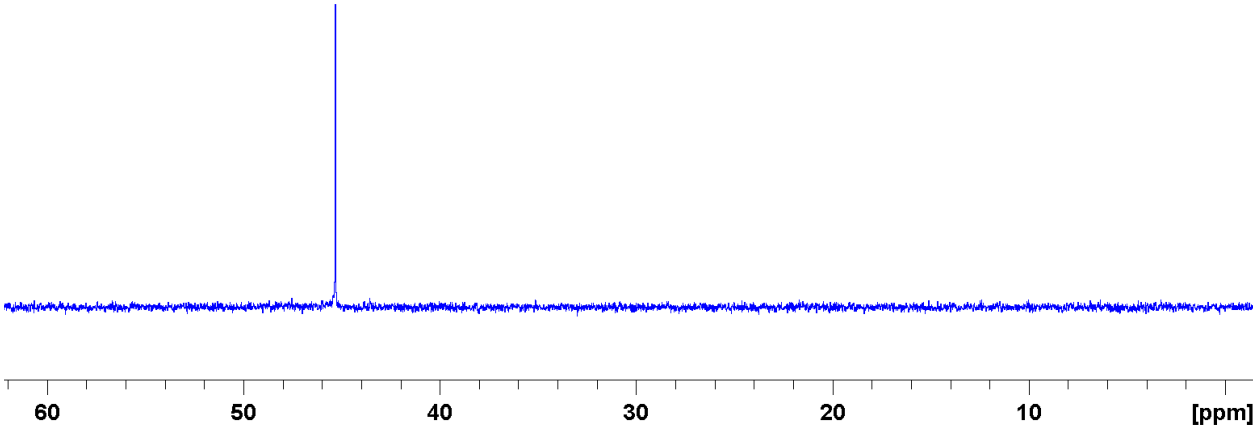

Figure S4. $^{31}P\{H\}$ NMR of **1a** in CD_3CN.

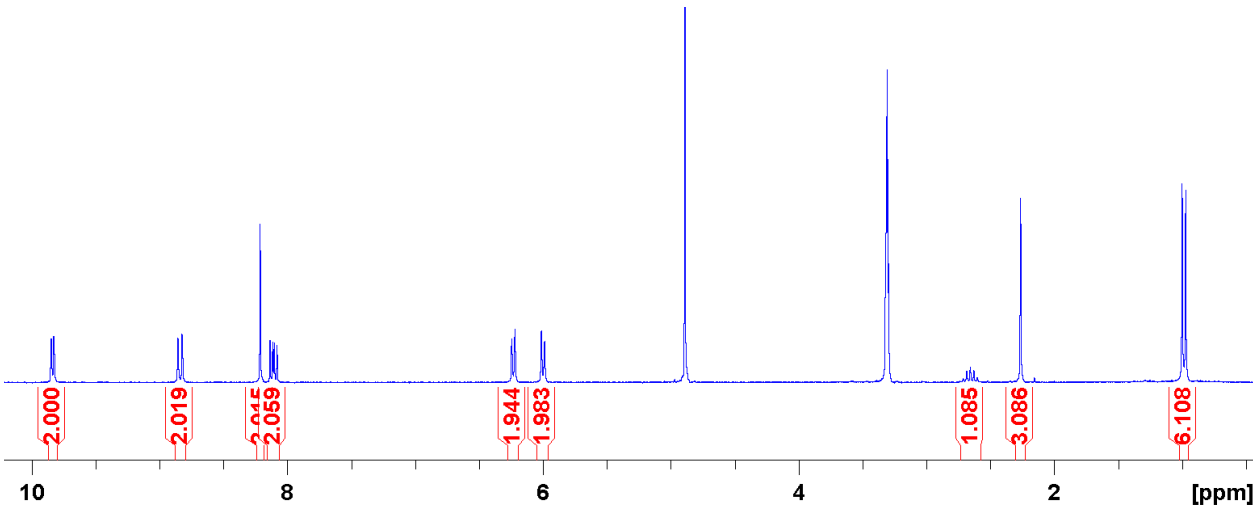

Figure S5. ^{1}H NMR of [Ru(p-cymene)(phen)Cl]Cl in CD_3OD.

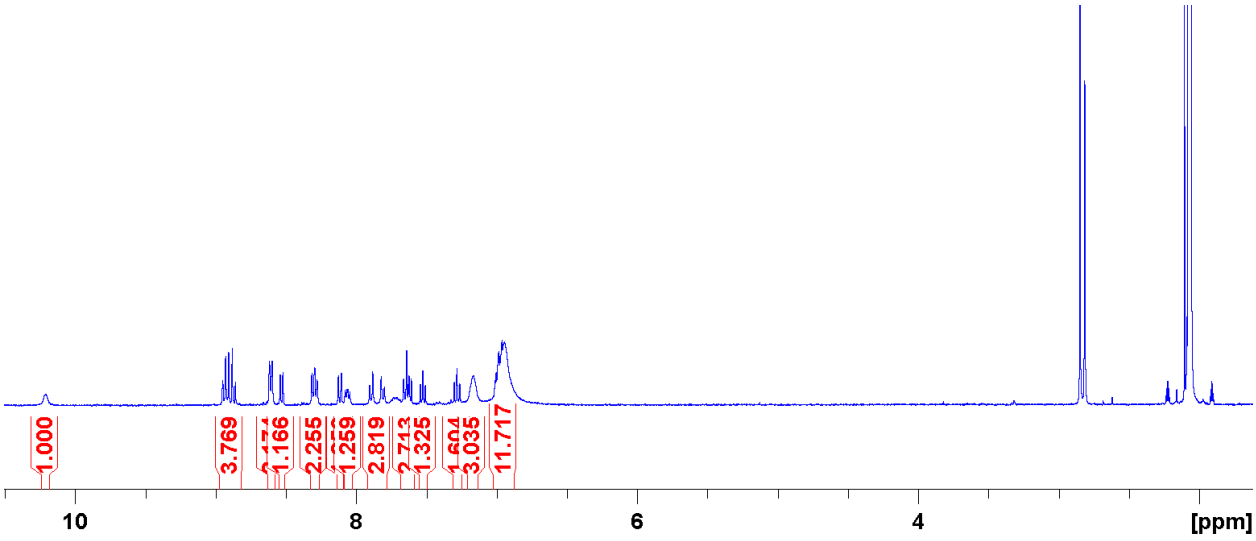

Figure S6. ^{1}H NMR spectrum of $[Ru(biq)(phen)(PPh_3)Cl]^{+}$ in $(CD_3)_2CO$.

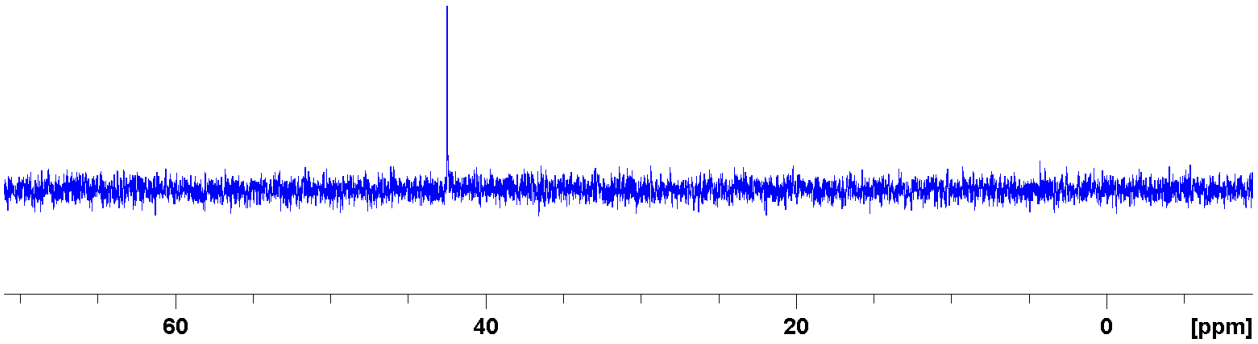

Figure S7. $^{31}P\{H\}$ NMR spectrum of $[Ru(biq)(phen)(PPh_3)Cl]^+$ in $(CD_3)_2CO$.

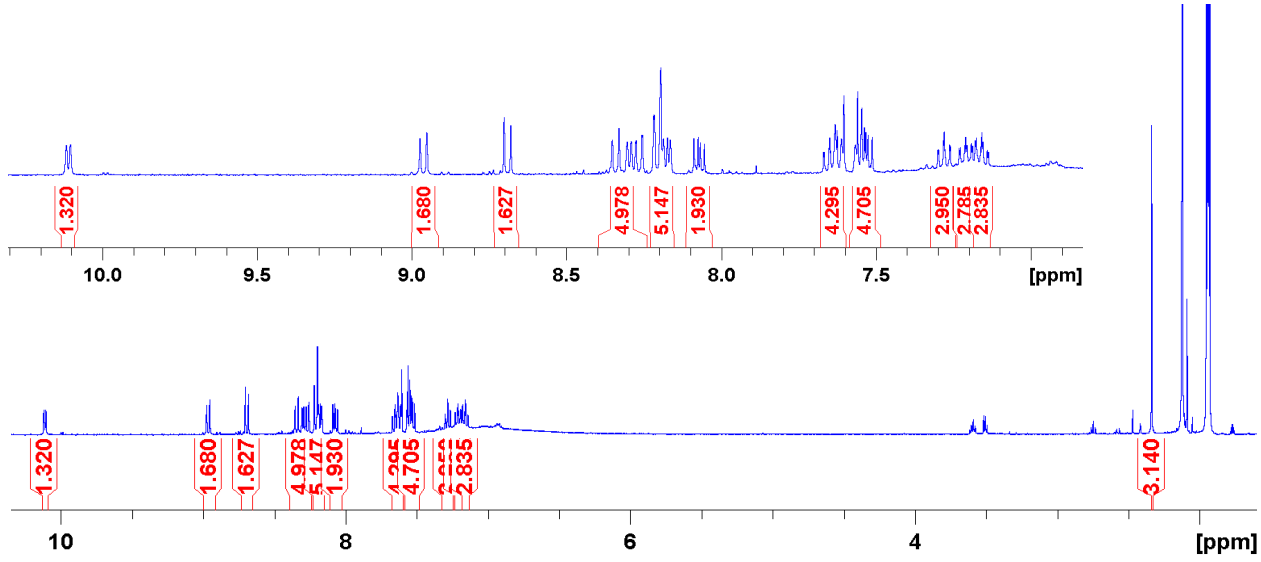

Figure S8. ^{1}H NMR of **2a** in CD_3CN.

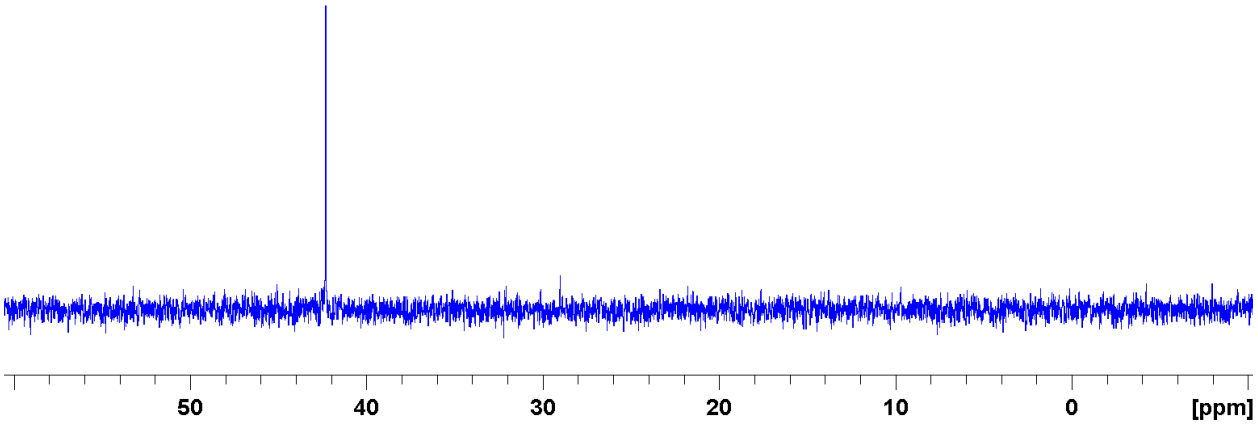

Figure S9. $^{31}P\{H\}$ NMR of **2a** in CD_3CN.

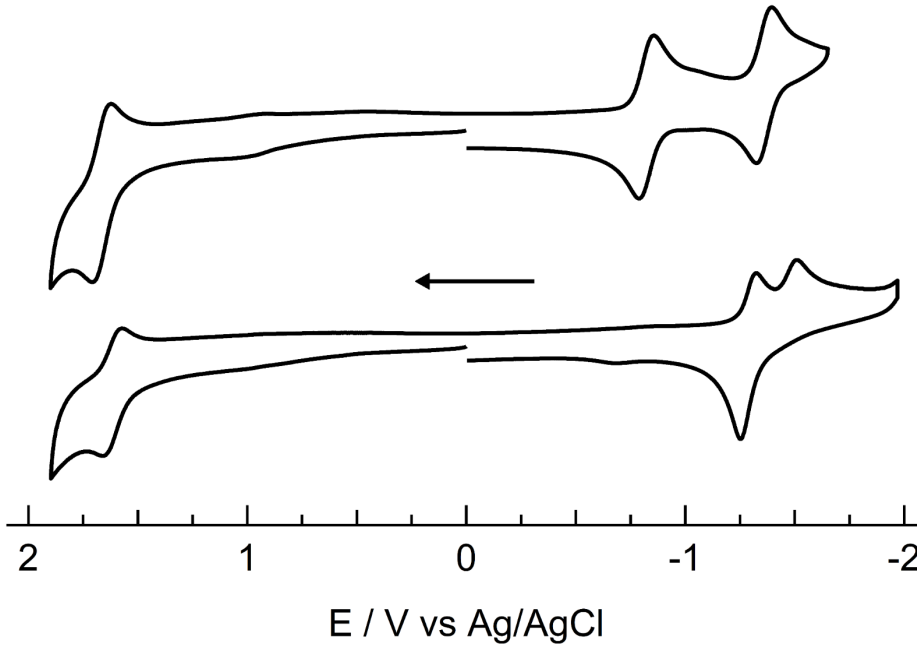

Figure S10. Circular Voltammograms of **1a** (top) and **2a** (bottom) in CH_3CN (0.1 M $TBAPF_6$).

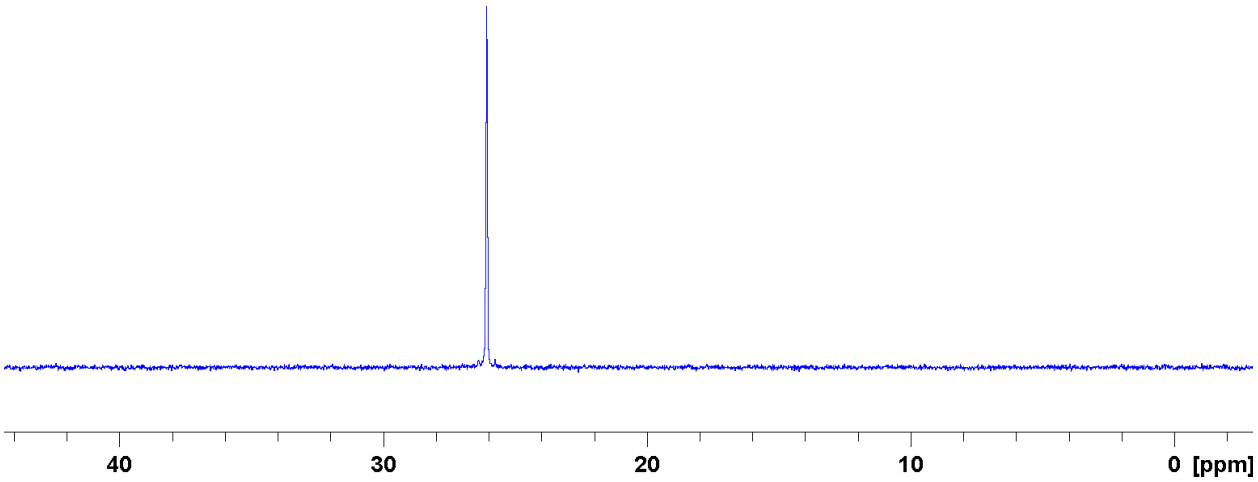

Figure S11. $^{31}P\{H\}$ NMR of $OPPh_3$ in CD_3CN.

Identification of Photolysis Intermediate I.

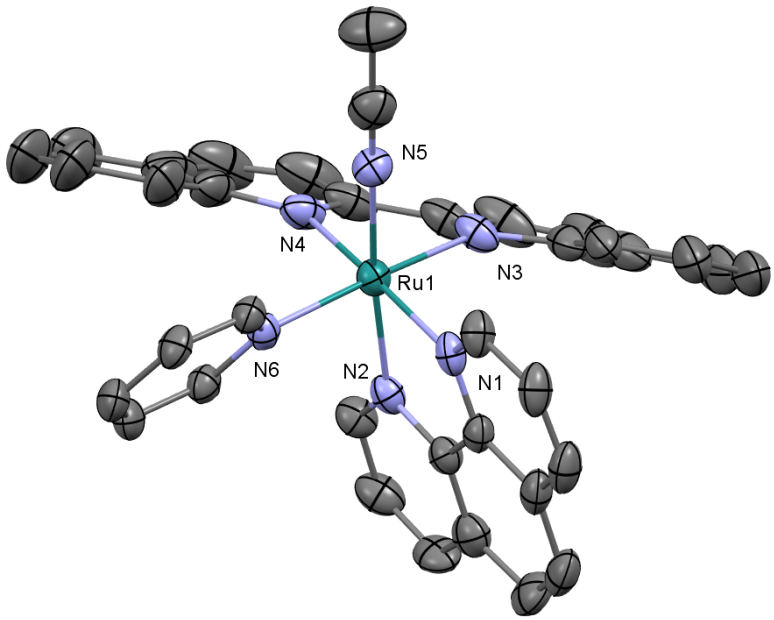

Figure S12. ORTEP plot of intermediate species $[Ru(biq)(phen)(py)(CH_3CN)]^{2+}$ (**I**) (thermal ellipsoids have been drawn at 50% probability and hydrogen atoms, PF_6^- molecules, and co-

crystallized solvent molecules have been omitted for clarity); Ru: cyan, N: light purple, and C: grey.

Table S1. Crystallographic data for intermediate species **I**.

Complex	$[Ru(biq)(phen)(py)(CH_3CN)]^{2+}$ (**I**)
Chemical formula	$RuC_{37}H_{28}F_{12}N_6P_2$
Formula weight	947.66
Temp (K)	100(2)
Crystal system	Triclinic
Space Group	P-1
a (Å)	10.7106(3)
b (Å)	12.0600(3)
c (Å)	17.6215(4)
α (°)	109.847(1)
β (°)	92.875(1)
γ (°)	103.835(1)
V ($Å^3$)	2057.24(9)
Z	2
D_{calc} (Mg/m^3)	1.530
Absorption coefficient (mm^{-1})	4.629
F(000)	948
Crystal size (mm)	0.25 x 0.137 x 0.072
Theta range for data collection (°)	2.694 to 74.926
Index ranges	$-13 \leq h \leq 13$
	$-15 \leq k \leq 15$
	$-21 \leq l \leq 22$
Reflections collected	54578
Unique reflections	8374 [R(int) = 0.0318]
Completeness to theta = 25.000°	99.7%
Data/restraints/parameters	8374 / 526 / 699
R1[a] (%) (all data)	0.0408 (0.0425)
wR2[b] (%) (all data)	0.1090 (0.1114)
Goodness-of-fit on F^2	1.052
Largest diff. peak and hole (e $Å^{-3}$)	0.870 and -0.390

[a]$R1 = \mathbf{\Sigma \mid |Fo|-|Fc| \mid / \Sigma |Fo| \times 100}$

[b]wR2 = $\mathbf{[\Sigma\, w\,(\,F_o^2\text{-}F_c^2\,)^2 \,/\, \Sigma\,(w\,|F_o|^2)^2]^{1/2}\ x\ 100}$

Spectral Deconvolution and Kinetic Analysis.

Analysis of the photolysis data for **2a** in pyridine was performed under the assumption of a consecutive chemical reaction of the type A → B → C. The data supported this assumption through the appearance of two sets of isosbestic points. For the conversion of A to B, isosbestic points report directly on the formation of C and were observed at 316, 448, and 500 nm. By contrast, direct information on the disappearance of A was garnered from B to C isosbestic points at 338, 361, and 550 nm.

The concentration of A and C were calculated directly from a linear combination of individual specie absorbance, Abs, at a fixed wavelength, λ, Eq. S1.

$$Abs_\lambda = b(\varepsilon_A^\lambda[A] + \varepsilon_B^\lambda[B] + \varepsilon_C^\lambda[C]) \quad \text{(S1)}$$

And

$$[A] + [B] + [C] = [C_t] \quad \text{(S2)}$$

Where ε_i is the extinction coefficient of the *i*th species at λ, b is the path length, and [A], [B], and [C] are molar concentrations of each component and C_t is the total concentration, *e.g.* the concentration of A initially present in solution. At a B to C isosbestic point,

$$\varepsilon_B^\lambda = \varepsilon_C^\lambda = \varepsilon_{BC}^\lambda \quad \text{(S3)}$$

Which allows simplification of Equation S1 into terms of [A],

$$[A] = \frac{Abs_\lambda - \varepsilon_{BC}^\lambda[C_t]}{\varepsilon_A^\lambda - \varepsilon_{BC}^\lambda} \quad \text{(S4)}$$

provided the extinction coefficient of the product, C, is known. At t = 20 min, it was assumed that the conversion of A to C was complete and ε_C was calculated from the initial concentration of **2a** (ε_{477} = 5,700 M^{-1} cm^{-1} in CH_3CN, [C_t] = 38.7 μM) used in the experiment, Figure S13.

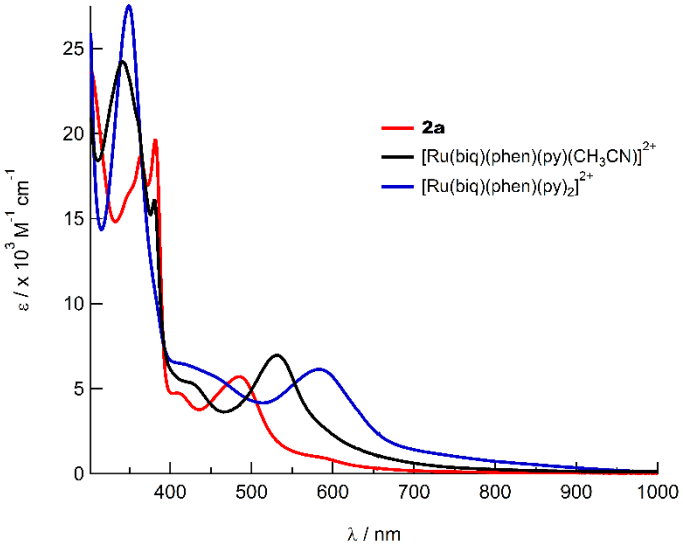

Figure S13. Extinction coefficient spectra of the three species observed during the photolysis of 2a (red line) in pyridine to form $[Ru(biq)(phen)(py)(CH_3CN)]^{2+}$ (black line), and $[Ru(biq)(phen)(py)_2]^{2+}$ (blue line).

The same approach was applied at the A to B isosbestic points which reports directly on the formation of C, except that

$$\varepsilon_A^\lambda = \varepsilon_B^\lambda = \varepsilon_{AB}^\lambda \quad \text{(S5)}$$

which results in the following expression

$$[C] = \frac{Abs_\lambda - \varepsilon_{AB}^\lambda [C_t]}{\varepsilon_C^\lambda - \varepsilon_{AB}^\lambda} \quad \text{(S6)}$$

for the concentration of C as a function of time. Relevant spectroscopic data for the isosbestic points used to determine [A] and [C] are given in Table S1. Once [A] and [C] were known, [B] B was calculated at each time point based from [C_t].

Table S2. Relevant Isosbestic Points, Reactions, and Extinction Coefficients Used In Spectral Deconvolution.

Isosbestic Point (nm)	Reaction	ε_C^{λ} (M^{-1} cm^{-1})	$\varepsilon_{AB}^{\lambda}$ (M^{-1} cm^{-1})	ε_A^{λ} (M^{-1} cm^{-1})	$\varepsilon_{BC}^{\lambda}$ (M^{-1} cm^{-1})
316	A to B	14,400	18,900	-	-
448	A to B	5,900	4,100	-	-
500	A to B	4,300	4,900	-	-
338	B to C	-	-	15,200	24,000
361	B to C	-	-	18,600	21,200
550	B to C	-	-	1,340	5,200

Note that the MLCT maxima for complex **2a** shifted to lower energy by ~10 nm (λ_{max} = 485 nm) when the solvent was changed from CH_3CN to pyridine. However, the extinction coefficient was assumed to be constant between these two points and 100% conversion to Ru(biq)(phen)$(py)_2$ was assumed in order to calculate the corresponding extinction coefficient spectrum. Finally, the extinction coefficient of Ru(biq)(phen)(py)(CH_3CN) was determined from Equation S7.

$$\varepsilon_B = \frac{A_o - \varepsilon_A[A] - \varepsilon_C[C]}{[B]} \quad \text{(S7)}$$

Numerical solutions to Equation S7 were determined at each time point from t = 0.25 to 10 min in order to collect an averaged, estimated extinction spectrum of Ru(biq)(phen)(py)(CH_3CN) which is shown in Fig S13.

Mole fractions of each component, χ_j, were calculated with Equation S8,

$$\chi_j = \frac{[j]}{[C_t]},\ j = [A], [B], [C] \quad \text{(S8)}$$

which were used as the data points of Figure 6 in the main text.

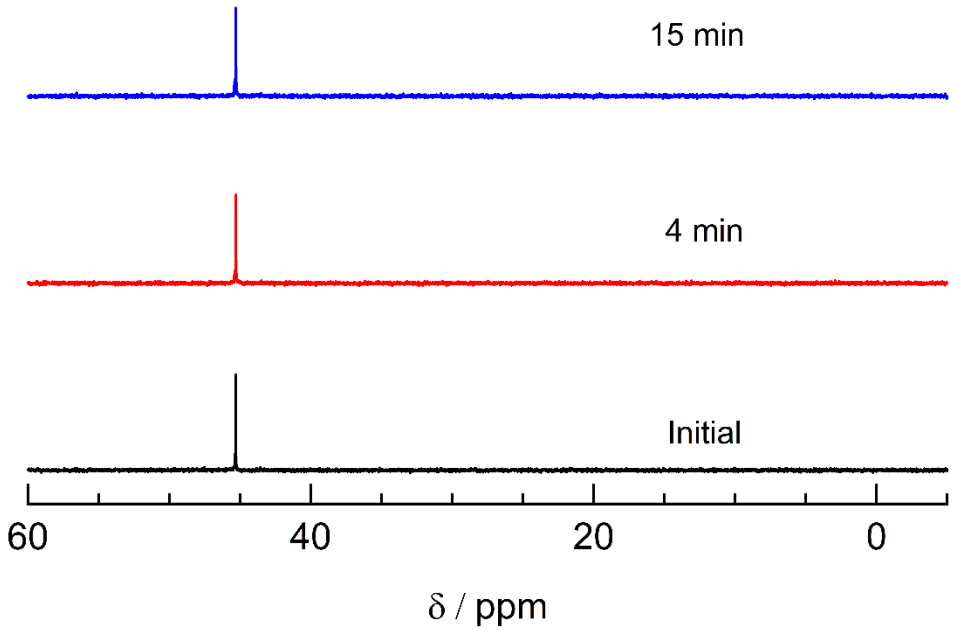

Figure S14. $^{31}P\{H\}$ NMR of **1a** as a function of irradiation time in CD_3CN ($\lambda_{irr} \geq 395$ nm).

Table S3. Crystallographic data for **1a**, **2a**, and **2b**.

Complex	**1a**	**2a**	**2b**
Chemical formula	$RuC_{51}H_{42}F_{12}N_5P_3$	$RuC_{52}H_{41}N_6F_{12}P_3$	$RuC_{34}H_{26}F_{12}N_6P_2$
Formula weight	1146.87	1171.89	909.62
Temp (K)	100.0	150(2)	100.0
Crystal system	Monoclinic	Triclinic	Triclinic
Space Group	P 1 21/n 1	P-1	P-1
a (Å)	17.6755(7)	12.2183(5)	10.2271(12)
b (Å)	13.6841(5)	13.9009(6)	11.7137(12)
c (Å)	21.4460(9)	15.8262(6)	14.9235(19)
α (°)	90	101.454(2)	97.547
β (°)	111.9850(1)	103.216(2)	100.062
γ (°)	90	91.967(2)	97.284
V ($Å^3$)	4810.0(3)	2555.73(18)	1724.4(3)
Z	4	2	2
D_{calc} (Mg/m^3)	1.584	1.523	1.752
Absorption coefficient (mm^{-1})	0.515	0.487	0.650
F(000)	2320	1184	908
Crystal size (mm)	0.279 x 0.223 x 0.148	0.19 x 0.15 x 0.08	0.253 x 0.216 x 0.054
Theta range for data collection (°)	2.851 to 26.396	3.001 to 28.298	2.804 to 26.411
Index ranges	$-22 \le h \le 20$	$-16 \le h \le 16$	$-12 \le h \le 12$
	$-17 \le k \le 17$	$-18 \le k \le 18$	$-14 \le k \le 14$
	$-26 \le l \le 26$	$-21 \le l \le 20$	$-18 \le l \le 18$
Reflections collected	47844	63494	48979
Unique reflections	9818 [R(int) = 0.0510]	12678 [R(int) = 0.0260]	7076 [R(int) = 0.0291]
Completeness to theta = 25.000°	99.8%	99.7%	99.8%
Data/restraints/parameters	9818 / 563 / 899	12678 / 253 / 768	7076 / 86 / 528
R1[a] (%) (all data)	3.81 (6.77)	2.97 (3.47)	2.72 (3.19)
wR2[b] (%) (all data)	8.29 (9.88)	7.68 (8.04)	6.76 (7.07)
Goodness-of-fit on F^2	1.050	1.047	1.062
Largest diff. peak and hole (e $Å^{-3}$)	0.722 and -0.557	0.649 and -0.478	0.537 and -0.388

[a]$R1 = \mathbf{\Sigma \, | \, |Fo|-|Fc| \, | \, / \, \Sigma \, |Fo| \times 100}$

[b]$wR2 = \mathbf{[\Sigma \, w \, (\, F_o^2-F_c^2 \,)^2 \, / \, \Sigma \, (w \, |F_o|^2)^2]^{1/2} \times 100}$

Table S4. Crystallographic and [1]GS calculated bond lengths and angles for **1a**, **2a**, and **2b**.

Bond angle (°)	**1a**		**2a**		**2b**	
	Expt.	**Calc.**	**Expt.**	**Calc.**	**Expt.**	**Calc.**
N1-Ru1-N2	80.1(1)	79.48	79.60(6)	78.98	79.54(7)	78.95
N1-Ru1-N3	87.7(2)	92.81	94.11(6)	93.57	100.22(7)	98.89
N1-Ru1-N4	166.3(5)	168.45	169.52(6)	168.79	172.15(7)	171.95
N1-Ru1-N5	94.6(1)	94.39	97.92(6)	96.32	94.34(7)	96.45
N1-Ru1-P1/N6	93.68(8)	91.80	85.23(4)	86.80	82.24(7)	83.92
N2-Ru1-N3	91.2(2)	88.87	81.96(6)	82.94	87.52(6)	86.24
N2-Ru1-N4	93.4(5)	92.72	94.71(6)	95.39	92.81(7)	93.42
N2-Ru1-N5	171.6(1)	172.04	174.21(6)	173.07	173.88(7)	175.02
N2-Ru1-P1/N6	93.41(8)	95.38	89.61(4)	89.06	87.70(7)	87.86
N3-Ru1-N4	80.3(5)	78.42	76.28(6)	76.01	77.54(7)	77.84
N3-Ru1-N5	82.1(2)	86.35	93.05(6)	92.34	93.52(7)	92.62
N3-Ru1-P1/N6	175.4(2)	174.23	171.51(4)	171.75	174.14(7)	172.85
N4-Ru1-N5	90.3(5)	92.55	86.91(6)	88.35	93.30(7)	91.07
N4-Ru1-P1/N6	98.8(4)	97.45	103.64(4)	102.91	99.31(7)	98.50
N5-Ru1-P1/N6	93.43(8)	89.84	95.42(4)	95.81	91.59(7)	93.60

Torsion angle (°)	**1a**		**2a**		**2b**	
	Expt.	**Calc.**	**Expt.**	**Calc.**	**Expt.**	**Calc.**
N1-C-C-N2	1.1(4)	0.96	2.1(2)	0.71	0.6(3)	0.89
N3-C-C-N4	2(1)	0.65	10.5(2)	9.98	3.1(3)	3.09

Bond lengths (Å)	**1a**		**2a**		**2b**	
	Expt.	**Calc.**	**Expt.**	**Calc.**	**Expt.**	**Calc.**
Ru1-N1	2.066(3)	2.0817	2.072(2)	2.0827	2.084(2)	2.0960
Ru1-N2	2.056(2)	2.0798	2.077(2)	2.0962	2.075(2)	2.0917
Ru1-N3	2.106(9)	2.1361	2.148(1)	2.1695	2.073(2)	2.1048
Ru1-N4	2.06(1)	2.1082	2.112(2)	2.1330	2.084(2)	2.0991
Ru1-N5	2.030(2)	2.0076	2.036(2)	1.9998	2.046(2)	2.0099
Ru1-P1/N6	2.343(1)	2.4105	2.3669(5)	2.4408	2.034(2)	2.0185

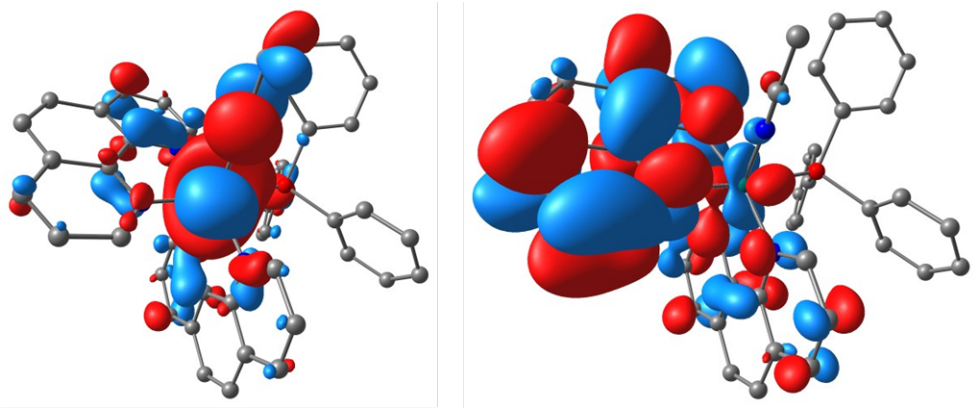

Figure S15. Electronic density plots of the calculated HOMO (left) and LUMO (right) of **1a** (drawn at isovalues of 0.02).

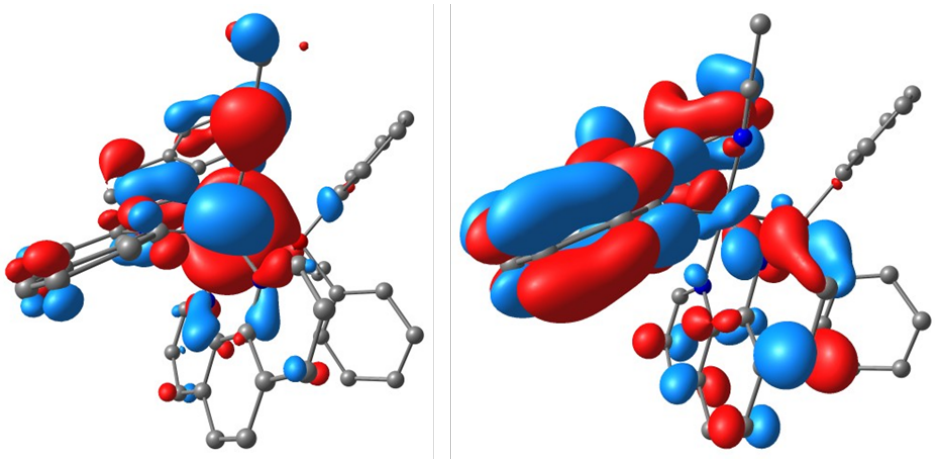

Figure S16. Electronic density plots of the calculated HOMO (left) and LUMO (right) of **2a** (drawn at isovalues of 0.02).

Table S5. Composition of Calculated HOMO and LUMO in **1a** and **2a**.

	1a		**2a**	
	HOMO	LUMO	HOMO	LUMO
Ru-d character (%)	77.3	2.60	71.2	3.25
CH_3CN (%)	7.97	0.21	7.98	0.44
PPh_3 (%)	3.27	0.75	1.84	1.24
phen (N1 and N2) (%)	5.62	10.4	4.30	11.0
biq/phen (N3 and N4) (%)	5.73	85.7	15.2	84.5

EC_{50} Curves

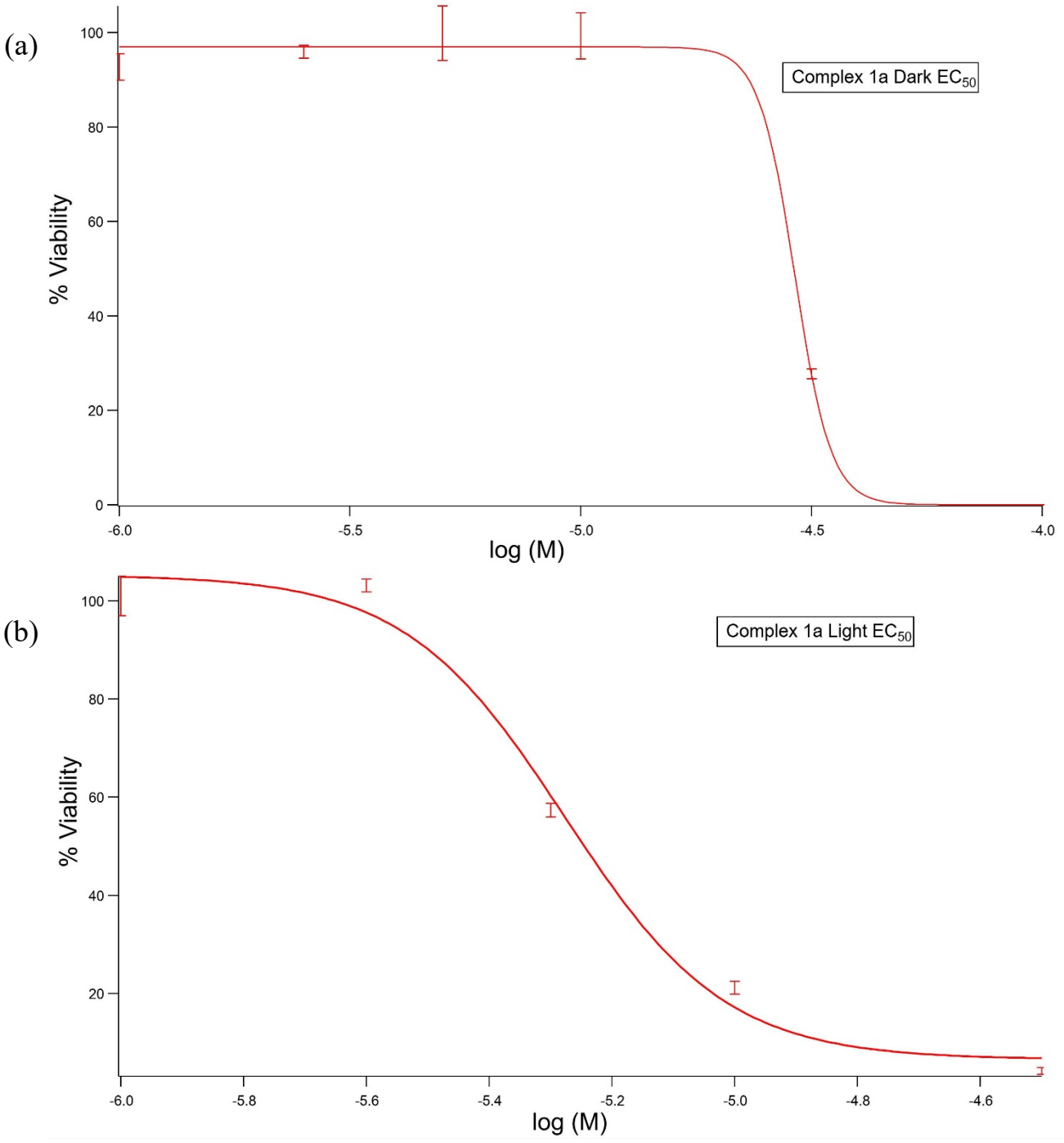

Figure S17. EC_{50} curves of **1a** (a) kept in the dark and (b) upon irradiation (t_{irr} = 20 min, λ_{irr} = 460–470 nm, 56 J/cm. Data are representative of three different experiments.

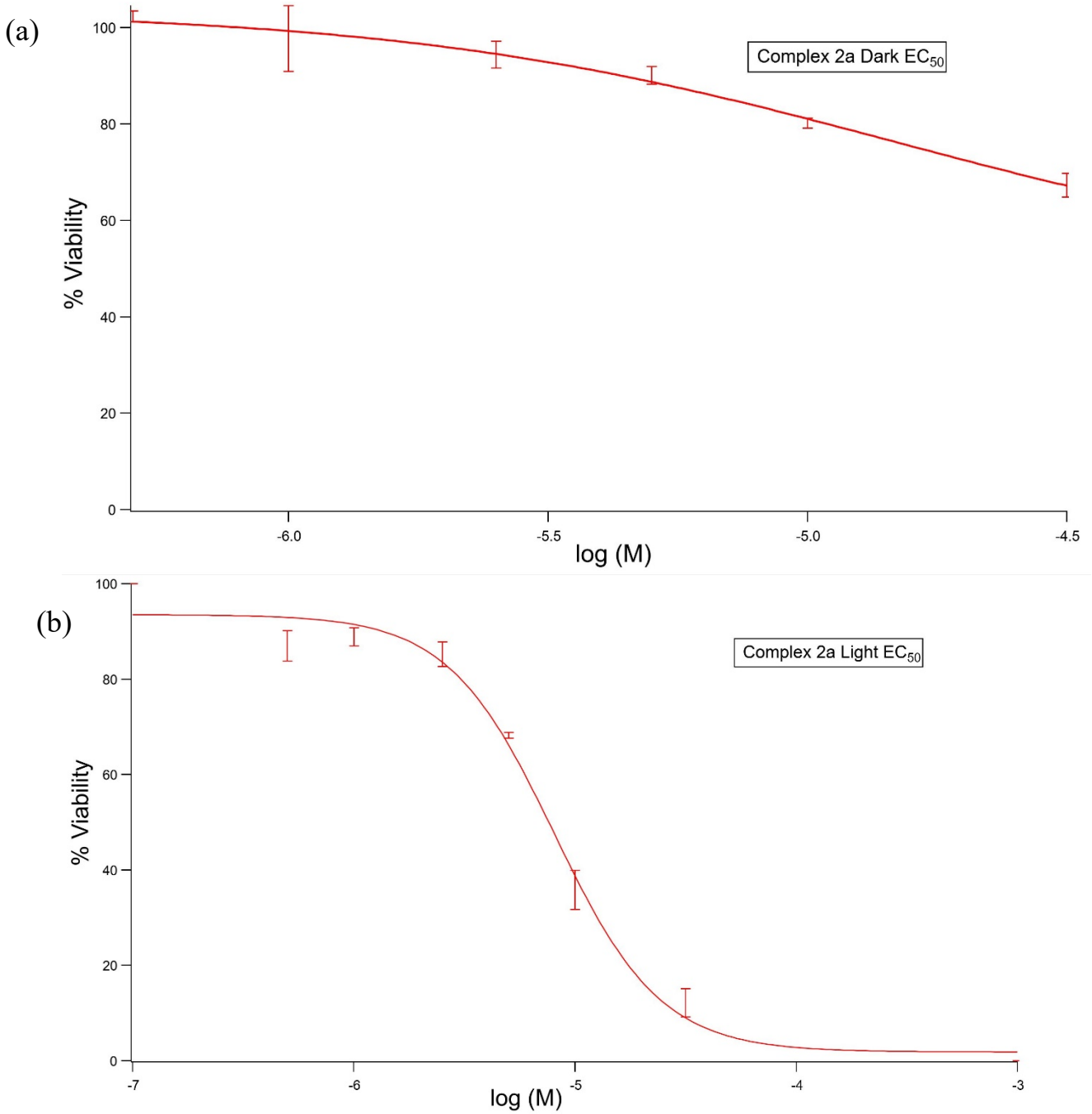

Figure S18. EC_{50} curves of **2a** (a) kept in the dark and (b) upon irradiation (t_{irr} = 20 min, λ_{irr} = 460–470 nm, 56 J/cm. Data are representative of three different experiments.

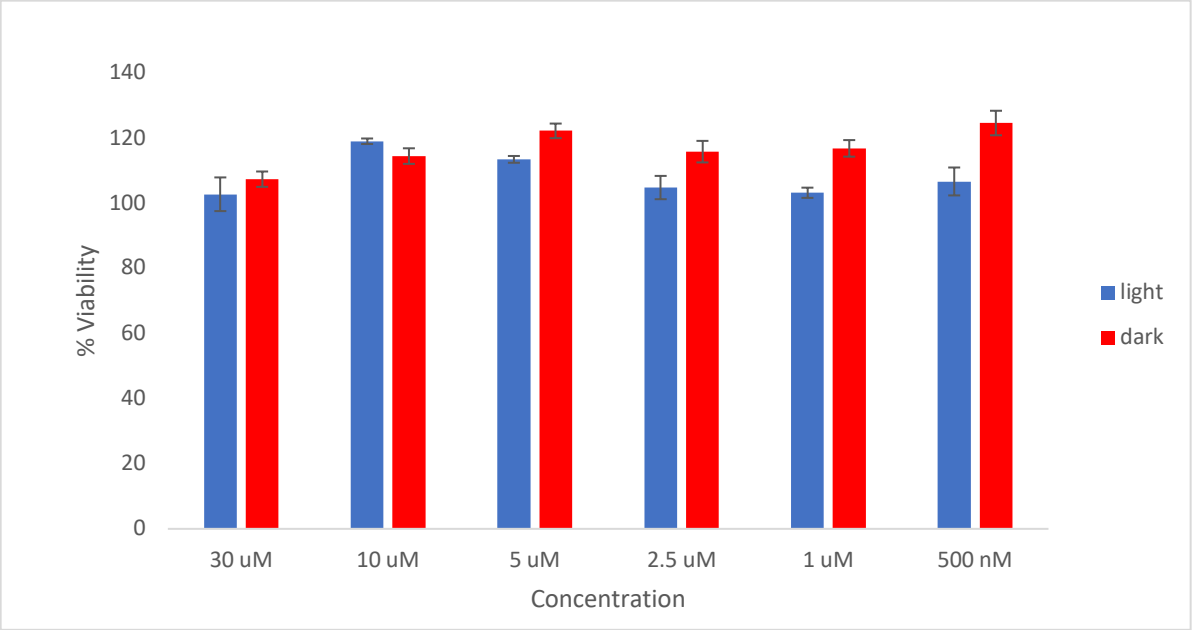

Figure S19. Viability of MDA-MB-231 cells when treated with DMEM supplemented with 10% FBS and 1,000 units/mL penicillin/streptomycin containing various concentrations of PPh_3 both in the dark and when irradiated with blue light (t_{irr} = 20 min, λ_{irr} = 460–470 nm, 56 J/cm^2).